PHYSICAL REVIEW FLUIDS **3**, 124305 (2018)

Multifractality of fine bubbles in turbulence due to lift

Itzhak Fouxon,[1,*] Gihun Shim,[2] Seulgi Lee,[2] and Changhoon Lee[1,2,†]
[1]*Department of Computational Science and Engineering, Yonsei University, Seoul 120-749, South Korea*
[2]*Department of Mechanical Engineering, Yonsei University, Seoul 120-749, South Korea*

(Received 22 January 2018; published 20 December 2018)

We develop a theory of spatial distribution of fine bubbles in turbulence and confirm it numerically. The bubbles are a few hundred microns in size and the considered value of the turbulence's strength is typical for oceans. The fluid applies a lift force on bubbles that causes bubble clustering by acting in a direction perpendicular to the rise velocity and the horizontal vorticity. We demonstrate that the centripetal attraction of bubbles to the cores of vortices is negligible compared with this effect. The combined action of the lift and the turbulence creates a continuum flow of bubbles distinct from the flow of the fluid and identical to the Peddley-Kessler (PK) model of swimming phytoplankton cells in the limit of strong gravitaxis. This allows one to derive a whole array of results by applying the theory of this model, which is well developed in the limit. The similarity explains the patchiness and clustering of bubbles in regions of downwelling flow; these properties are understood for motile phytoplankton. The bubble clustering decreases the average rise velocity, prolonging the time until the bubble's rupture at the surface. We demonstrate that bubbles form columnar structures characterized by a multifractal distribution with the dimension deficit increasing as the eighth power of the radius. Fractal dimensions are derived from the information dimension given by the Kaplan-Yorke formula. We also provide some results for the shape-dependent PK model. We confirm the theory by direct numerical simulations of the bubbles' motion in Navier-Stokes turbulence.

DOI: 10.1103/PhysRevFluids.3.124305

I. INTRODUCTION

Bubbles are ubiquitous in water and influence the physics and biology of oceans in many ways. These include interactions with microorganisms, aeration, gas exchange with the atmosphere, mixing, and production of stresses at the air-ocean interface by rupture. Collisions with microorganisms can be critical for the healthy functioning of the ecosystems, causing oxygenation. They can also be harmful, creating stresses on the organisms' surfaces (see the review in [1] and the references therein). Artificial aeration is well known for its beneficial ecological effects, including prevention of fish kills due to low dissolved oxygen concentrations [2]. Ocean flows are typically turbulent, which makes an understanding of bubbles' behavior in turbulence practically relevant.

Bubble-laden turbulence has been studied for a long time [3–13]. The importance of the lift force in the equation of motion of the bubble [14,15] was first recognized in [5]. Bubbles were found to accumulate on the downward side of vortices due to this force. The accumulation implies a decrease in the rise velocity of the bubble [7–9]. A segregation indicator was proposed to characterize the particle distribution [10] and the Lagrangian acceleration statistics of the bubbles were measured [13]. It was proposed that bubbles form multifractals similarly to light inertial particles that are

*itzhak8@gmail.com
†clee@yonsei.ac.kr

trapped by vortex cores [11,12]. Recently, the behavior of bubbles in rotating turbulence was studied numerically [16].

One of the main contributions of this paper is the demonstration that the centripetal attraction of bubbles to the cores of vortices is negligible in the usually used equation of motion of the bubble, which is dominated by the lift force. The familiar bubble clustering in the downflow regions is solely due to the lift (cf. [7]). We prove that the equation of motion implies that fine bubbles in dilute solution are distributed over a multifractal set characterized by a log-normal coarse-grained concentration. This set is the attractor of the effective continuum dynamics of the bubbles. The lift force pushes the bubbles in regions of downwelling flow. We provide formulas for the fractal dimensions and the Lyapunov exponents in terms of the energy spectrum of Navier-Stokes turbulence. The preferential concentration of bubbles in the regions of downwelling flow is described by negative cross correlations of the vertical component of the turbulent flow with the bubbles' flow divergence and concentration. The cross correlation with the concentration also determines the value of the negative turbulence correction to the average rise velocity of the bubble. We provide the radial distribution function (RDF), which gives the probability of finding another bubble at a given distance from the considered particle. The RDF determines the evolution of the size distribution of bubbles due to their collisions and coalescence [17]. The predictions hold for bubbles in Navier-Stokes turbulence and are validated by direct numerical simulations (DNSs).

The key observation underlying the above results is that after transients, the bubble's velocity is determined uniquely by the local flow and vorticity. This provides the bubbles' counterpart of the famous Maxey formula for the velocity of the weakly inertial particle [18]. However, in contrast with the inertial particles, where there is a regime of large inertia in which the flow description breaks down (see, e.g., [19–22]), here the flow description is valid over the whole range of validity of the equation of motion. Remarkably, the bubble velocity coincides in form with the velocity of motile phytoplankton cells (for example, *H. akashivo* considered in [23]) in the Pedley-Kessler (PK) model in the limit of slow flow [23–26]. We find a one-to-one correspondence of parameters of motion for these two problems. The rise velocity of the bubble corresponds to the swimming velocity of the cell and the lift force corresponds to the gyrotactic term. Thus, we can apply the well-developed theory of the steady-state behavior of motile phytoplankton in homogeneous turbulence to bubbles by renaming the parameters. We observe that the correspondence is not sensitive to small refinements of the equation of motion. These refinements could become necessary because the Reynolds number of the perturbation flow is finite, and the theories involve phenomenological descriptions.

The theory of motile phytoplankton distribution in turbulence assumes that the velocity of the phytoplankton cell is the sum of the local turbulent velocity and the swimming velocity of the cell, as proposed by the PK model [23–27]. This swimming velocity is usually much smaller than the velocity of the flow. This is why motile phytoplankton cells in turbulence can for some purposes be treated as passive tracers similar to nonmotile species (for example, diatoms). In the steady state, passive tracers would be distributed uniformly in a finite volume. However, the distribution of motile phytoplankton is observed to be inhomogeneous [23,25]. This inhomogeneity is due to the small swimming velocity, which constitutes a singular perturbation of the incompressible turbulent flow of passive tracers. The motility, despite the fact that it is an active property of the cell, can in limiting cases be "enslaved" by the turbulence. The particle velocity becomes a passive property that is determined completely by the local flow and its first derivatives. Thus, the velocity, through the flow and its derivatives, is a function of the particle position, allowing one to define the spatial flow of the cells [23]. This flow is detached from the fluid and, in contrast to incompressible fluid flow, has a small but finite compressibility. The accumulation of the effects of the compressibility with time results in a spatial distribution that is multifractal rather than uniform. The distribution is supported on a time-dependent attractor that can be described in detail using the theory of distributions of particles transported by an arbitrary weakly compressible random flow [12,19] (see also [27]). This was used to predict the fractal dimensions in [23]. The result for the dimensions was refined in [26], where it was demonstrated that some of the observations of [23] in fact belonged to a different regime (cf. [28]). Further predictions were also made in [26], including the demonstration that the mean turbulent velocity in the frame of the cell is negative. This provided a quantitative description of the preferential concentration of microorganisms in downwelling flow. A study of nonspherical gyrotactic microswimmers was performed in [27,28].

It must be stressed that the above phenomena occur at the smallest scales of turbulent flow: The multifractality holds below the viscous scale of turbulence. On larger scales, the coarse-grained concentration is constant in the steady state. The familiar paradigm where plankton's concentration is considered as a passive scalar mixed by turbulence applies. Collisions of particles occur on the scale of particles and are often influenced appreciably by small-scale multifractality (see, e.g., [19]).

We stress that the validity of the PK model for the description of the motion of swimmers is irrelevant for our results. We are simply using known results of the study of this mathematical model. We confirm the correspondence by DNSs of the equation of motion of bubbles in turbulence.

Our work is in line with a whole array of recent works that derive from the observation that the velocity of a certain small particle in turbulence is determined uniquely by its position. In this case, the velocities of spatially close particles are almost equal and therefore one can introduce continuum spatial flow of particles. This flow, in contrast with incompressible flow of fluid, is compressible, leading to clustering of particles. The compressibility, however, is weak, allowing one to apply the general theory of transport by smooth weakly compressible flow [12]. This theory was corroborated in many cases, including inertial particles, tracers transported by surface wave turbulence, motile phytoplankton cells, inertial particles under gravity, and phoretic particles [12,19,23,26,29–33]. Among the described cases, the case of motile phytoplankton stands out as it pertains to a living organism. It would be interesting to consider whether other cases of clustering of living organisms in turbulence can also be described within this framework. Clustering of flocking particles observed in [34–36] is a possibility.

The next section is the core of this paper. We derive a reduction of the usual equation of motion of an isolated bubble in turbulence. The reduction holds over the whole range of validity of the equation and has the form of the reduced PK model. The PK model and its reduction are presented in Sec. III. The reduced form is ready for application of the general theory of clustering in weakly compressible flows, which is performed in Sec. IV. Section V reports the results of the DNS of the original equation of motion of the bubble in Navier-Stokes turbulence. The results agree with the predictions made by using the reduced equation of motion. In Sec. VI we provide a brief overview and consider open questions.

II. REDUCTION OF A BUBBLE'S EQUATION OF MOTION

The equation of motion of a spherical bubble with radius a in an incompressible turbulent flow $\boldsymbol{u}(t, \boldsymbol{x})$ is

$$\dot{\boldsymbol{v}} = 3[\partial_t \boldsymbol{u} + (\boldsymbol{u} \cdot \nabla)\boldsymbol{u}] - \frac{\boldsymbol{v} - \boldsymbol{u} - \boldsymbol{v}_g}{\tau} + \boldsymbol{\omega} \times (\boldsymbol{v} - \boldsymbol{u}) \tag{1}$$

(see [7,8] and the references therein). Here $\boldsymbol{v}(t)$ is the bubble's velocity, $\boldsymbol{\omega} = \nabla \times \boldsymbol{u}$ is the vorticity, and $\boldsymbol{v}_g = -2\boldsymbol{g}\tau$ is the bubble rise velocity in still fluid. The gravitational acceleration $\boldsymbol{g}$ is directed along the negative z axis. The flow and its derivatives are taken at the position of the particle $\boldsymbol{x}(t)$. We assume that bubbles are rare in the flow and therefore both hydrodynamic interactions of the bubbles and the bubbles' reaction on the flow can be neglected (one-way coupling).

The range of validity of Eq. (1) is determined by the form of the lift force given by the last term of the equation. It uses the lift force coefficient 0.5, which is valid at $1 \sim \mathrm{Re} \lesssim 100$ (see [7,8,14,15]). Thus, the Reynolds number $\mathrm{Re} = 2|\boldsymbol{v} - \boldsymbol{u}|a/\nu$ of the flow perturbation caused by the bubble is not small. Nevertheless, we use the linear form of the drag force, which is typical for the small Re case. The effect of finite Re is described by introducing in the relaxation time $\tau = a^2/6\nu r$ the Reynolds-dependent numerical factor $r = 1 + 0.15\,\mathrm{Re}^{0.687}$, where ν is the kinematic viscosity. Somewhat different phenomenological descriptions of the drag are also possible (see [7,29] and the references therein). The effective description of the drag applies at $\mathrm{Re} \lesssim 100$, which includes the range of validity of the form of the lift force. We have $r \sim 1$ over the whole range; however, $6r$ appearing in τ can be of order 10 and must be retained in the estimates.

We used the form of the drag of rigid particles, where the fluid obeys the no-slip boundary condition on the particle's surface. This approximation is usually valid because the impurities present in the fluid accumulate at the bubble's surface, making it effectively rigid. Thus, experiments demonstrate that the behavior of these bubbles is similar to that of rigid particles [37,38], and bubbles in water in the size range 10–300 μm can be described as rigid [39]. Larger, clean, and fully recirculating spheres that would violate the no-slip boundary conditions can occur; however, they are not typical in the size range considered here (50–400 μm, discussed below) [39]. In those cases where the rigidity assumption is violated, other forms of the drag force must be used; however, this would not change the following conclusions much. Finally, as far as the form of the lift force is concerned, the rigidity of the surface is less relevant because the force's derivation relies only on the condition of the zero normal component of the flow at the surface [14].

The remaining terms on the right-hand side (RHS) of Eq. (1) represent the fluid acceleration plus the added mass effects and the buoyancy [7,8]. We use the form of the added mass term from [40] that slightly corrects [41] (see [3]). The equation assumes that a is much smaller than the smallest length of turbulence [42], the Kolmogorov scale η. Thus, the Stokes number $\mathrm{St} \equiv \tau/\tau_\eta = a^2/6r\eta^2$, measuring inertia, obeys $\mathrm{St}^{1/2} \ll 1$. Here $\tau_\eta = \eta^2/\nu = \sqrt{\nu/\epsilon}$ is the viscous time and ϵ is the energy dissipation rate per unit volume of the fluid [42]. We conclude that the inertia of the bubble is always small in the domain of validity of Eq. (1).

We demonstrate that the bubble's drift velocity with respect to the flow $\boldsymbol{v} - \boldsymbol{u}$ is approximately given by the rise velocity in still fluid $\boldsymbol{v}_g$. Indeed, the drift is composed of $\boldsymbol{v}_g$ and the inertial drift velocity $\tau[\partial_t \boldsymbol{u} + (\boldsymbol{u} \cdot \nabla)\boldsymbol{u}] \sim \mathrm{St}\eta/\tau_\eta$ that holds at small St and negligible gravity [18]. The order of magnitude of the drift velocity is given by the larger of the two contributions, as can be confirmed by considering the bubble's velocity after transients

$$\boldsymbol{v}(t) - \boldsymbol{u}[t, \boldsymbol{x}(t)] = \boldsymbol{v}_g + \int_{-\infty}^{t} \exp\left[-\frac{t-t'}{\tau}\right]\Bigg(3[\partial_t \boldsymbol{u} + (\boldsymbol{u}\cdot\nabla)\boldsymbol{u}][t', \boldsymbol{x}(t')] + \frac{\boldsymbol{u}[t', \boldsymbol{x}(t')] - \boldsymbol{u}[t, \boldsymbol{x}(t)]}{\tau} + \boldsymbol{\omega}[t', \boldsymbol{x}(t')] \times \{\boldsymbol{v}(t') - \boldsymbol{u}[t', \boldsymbol{x}(t')]\}\Bigg)dt', \tag{2}$$

obtained by integrating Eq. (1). The last term in the integrand is St times smaller than $|\boldsymbol{v} - \boldsymbol{u}|$ and can be neglected. The resulting integral is of order $\mathrm{St}\eta/\tau_\eta$. We observe that if we had $\mathrm{St}\eta/\tau_\eta \gtrsim v_g$, then Re would be of order $(a/\eta)\mathrm{St}$ and could not be larger than one as required by the validity of Eq. (1). We conclude that the necessary condition for the validity of the equation is $v_g \gg \mathrm{St}\eta/\tau_\eta$ and, correspondingly, $\boldsymbol{v}(t) - \boldsymbol{u}[t, \boldsymbol{x}(t)] \approx \boldsymbol{v}_g$.

The constant drift velocity implies that the drag is linear in the particle velocity. Indeed, the Reynolds number of the flow perturbation due to the bubble is constant, $\mathrm{Re} = 2av_g/\nu$. This implies that the r factor in the definition of τ is also constant. The drag is given by the constant relaxation time $\tau = a^2/6\nu r$.

The validity of Eq. (1) depends on gravity: The equation breaks down in the zero-gravity limit. This is because without gravity we cannot make the conditions of small inertia and nonsmall Re consistent. The condition governing the magnitude of the gravity can be expressed in terms of the dimensionless Froude number $\mathrm{Fr} = \epsilon^{3/4}/g\nu^{1/4}$. This number gives the ratio of the typical turbulent acceleration $\epsilon^{3/4}/\nu^{1/4}$ and g and must be very small for the equation to be valid. Indeed, $\mathrm{Re} \gtrsim 1$ gives $g \gtrsim \nu^2/a^3$, where ν^2/a^3 can be written as $(6r\,\mathrm{St})^{-3/2}$ times $\epsilon^{3/4}/\nu^{1/4}$. Because $\mathrm{St}^{1/2} \ll 1$, we conclude that g must be at least three orders of magnitude larger than the turbulent acceleration $\mathrm{Fr} \lesssim 10^{-3}$.

The Reynolds number of the flow perturbation due to the bubble is determined uniquely by the bubble radius, $\mathrm{Re} = 2ga^3/3\nu^2 r$. Using the water viscosity $\nu = 10^{-6}$ m^2/s, we find that the range $1 \lesssim \mathrm{Re} \lesssim 100$ corresponds to bubble radii from approximately 50 to 400 μm. This range of the radii is smaller than the Kolmogorov scale for typical turbulent dissipation rates, $\epsilon \simeq 10^{-8}$–10^{-6} m^2/s^3, holding in the ocean. Indeed, the smallest η that is reached for $\epsilon \simeq 10^{-6}$ m^2/s^3 is approximately 1000 μm. We conclude that Eq. (1) applies to fine bubbles with a size of 50–400 μm. This range overlaps significantly with the range of bubble sizes of 20–200 μm observed in the ocean [43,44].

We demonstrate that flow gradients in the frame of the bubble, $\nabla_k u_i[t, \boldsymbol{x}(t)]$, change due to the sampling of different spatial regions of the flow by the rising bubble and not due to the temporal evolution of turbulence. For the bubble that rises through the turbulent velocity field $\boldsymbol{v}(t = t_0, \boldsymbol{x})$ at a fixed time t_0, the gradients change in its frame in the characteristic time $\tau_g = \eta/v_g$. Indeed, this is the time during which the bubble crosses the spatial correlation length η of the turbulent velocity gradients. This time is much smaller than the time τ_η of variations of gradients in the frame of the fluid particle: $\tau_\eta/\tau_g = 2\,\mathrm{St}/\mathrm{Fr} = \mathrm{Re}\eta/2a \gg 1$. Considering now the motion of the bubble in the full time-dependent flow, the gradients of the flow are conserved in the frame of the fluid particle over times of order τ_g. However, during this time, the bubble would separate from the fluid particle by the distance η and see a spatial region with different gradients. We conclude that the flow gradients change over time τ_g in the frame of the bubble.

Remarkably, the arising hierarchy of timescales corresponds to the overdamped limit, which allows us to reduce the equation of motion. The ratio $\tau/\tau_g = \mathrm{Re}a/12r\eta$ increases with Re. Its maximal value of $1.8a/\eta$ is attained at $\mathrm{Re} = 100$ and is much smaller than one. Thus, the overdamped limit $\tau \ll \tau_g \ll \tau_\eta$ holds in the domain of validity of Eq. (1). Because τ is much smaller than the time of variations of the term in large square brackets in Eq. (2), the integral is determined by a small vicinity of t of order τ. It can be obtained using the Taylor expansion of the integrand in $t - t'$. We find

$$\boldsymbol{v}(t) \approx \boldsymbol{u}[t, \boldsymbol{x}(t)] + \boldsymbol{v}_g + 2\tau[\partial_t \boldsymbol{u} + (\boldsymbol{u}\cdot\nabla)\boldsymbol{u}] - \tau(\boldsymbol{v} - \boldsymbol{u})\cdot\nabla\boldsymbol{u} - \tau(\boldsymbol{v} - \boldsymbol{u})\times\boldsymbol{\omega}. \tag{3}$$

Iterating this once, we find that the motion of the particles can be described by smooth spatial flow:

$$\frac{d\boldsymbol{x}}{dt} = \boldsymbol{v}[t, \boldsymbol{x}(t)], \quad \boldsymbol{v}(t, \boldsymbol{x}) = \boldsymbol{u}(t, \boldsymbol{x}) + \boldsymbol{v}_g - \tau\boldsymbol{v}_g \times \boldsymbol{\omega} + 2\tau[\partial_t \boldsymbol{u} + (\boldsymbol{u}\cdot\nabla)\boldsymbol{u}] - \tau(\boldsymbol{v}_g\cdot\nabla)\boldsymbol{u}. \tag{4}$$

This flow is the bubbles' counterpart of Maxey's [18] formula (5.7) for the flow $\boldsymbol{v}^i$ of inertial particles $\boldsymbol{v}^i = \boldsymbol{u} + \boldsymbol{v}_g^p - \tau^p[\partial_t \boldsymbol{u} + (\boldsymbol{u}\cdot\nabla)\boldsymbol{u}] - \tau^p(\boldsymbol{v}_g^p\cdot\nabla)\boldsymbol{u}$. Here $\boldsymbol{v}_g^p = \boldsymbol{g}\tau^p$ is the settling velocity of the particle and τ^p is the Stokes time. The difference between the two formulas is the reversal of the sign before the $\partial_t \boldsymbol{u} + (\boldsymbol{u}\cdot\nabla)\boldsymbol{u}$ term in the last line of Eq. (4): The bubbles cluster in vortices, but inertial particles cluster outside the vortices. This is readily seen by observing that $2\tau[\partial_t \boldsymbol{u} + (\boldsymbol{u}\cdot\nabla)\boldsymbol{u}]$ contributes $2\tau\nabla_k u_i \nabla_i u_k$ to the flow divergence. Because $\nabla_k u_i \nabla_i u_k$ is approximately the difference between the local strain and the vorticity, the divergence $2\tau\nabla_k u_i \nabla_i u_k$ is negative in vortices. Thus, the centripetal attraction of bubbles to the cores of the vortices is described. Further, the difference between $\boldsymbol{v}$ and $\boldsymbol{v}^i$ is the last vorticity term in Eq. (4) and has no counterpart in inertial particles; it is considered below.

It is a well-established fact that because of the centrifugal acceleration, inertial particles cluster in strain regions and light particles cluster in vortices. Thus, one might think that bubbles cluster in vortices similarly to light particles (see, e.g., [12]). However, this is not the case. We consider the full divergence of the flow defined in Eq. (4):

$$\nabla\cdot\boldsymbol{v} = 2\tau\nabla_k u_i \nabla_i u_k - 2g\tau^2\nabla^2 u_z. \tag{5}$$

The ratio of the last term in $\nabla\cdot\boldsymbol{v}$ to the first one is $\mathrm{St}/\mathrm{Fr} \gg 1$. A similar ratio holds for the corresponding contributions in the flow. We conclude that the $2\tau[\partial_t \boldsymbol{u} + (\boldsymbol{u}\cdot\nabla)\boldsymbol{u}]$ term in Eq. (4) can be neglected, giving

$$\boldsymbol{v} \approx \boldsymbol{u} + \boldsymbol{v}_g - \tau\boldsymbol{v}_g \times \boldsymbol{\omega} = \boldsymbol{u} + (\tau v_g \omega_y, -\tau v_g \omega_x, v_g), \quad \nabla\cdot\boldsymbol{v} \approx -2g\tau^2\nabla^2 u_z. \tag{6}$$

We neglected the last term in Eq. (4) because corrections to $\boldsymbol{v} \approx \boldsymbol{u} + \boldsymbol{v}_g$ are small in terms of absolute value. They are relevant only if they exhibit finite divergence, because that vanishes in the leading order. The compressibility, however small it is, can bring an order-one clustering effect over a long evolution time, which is why small terms with finite compressibility must be retained.

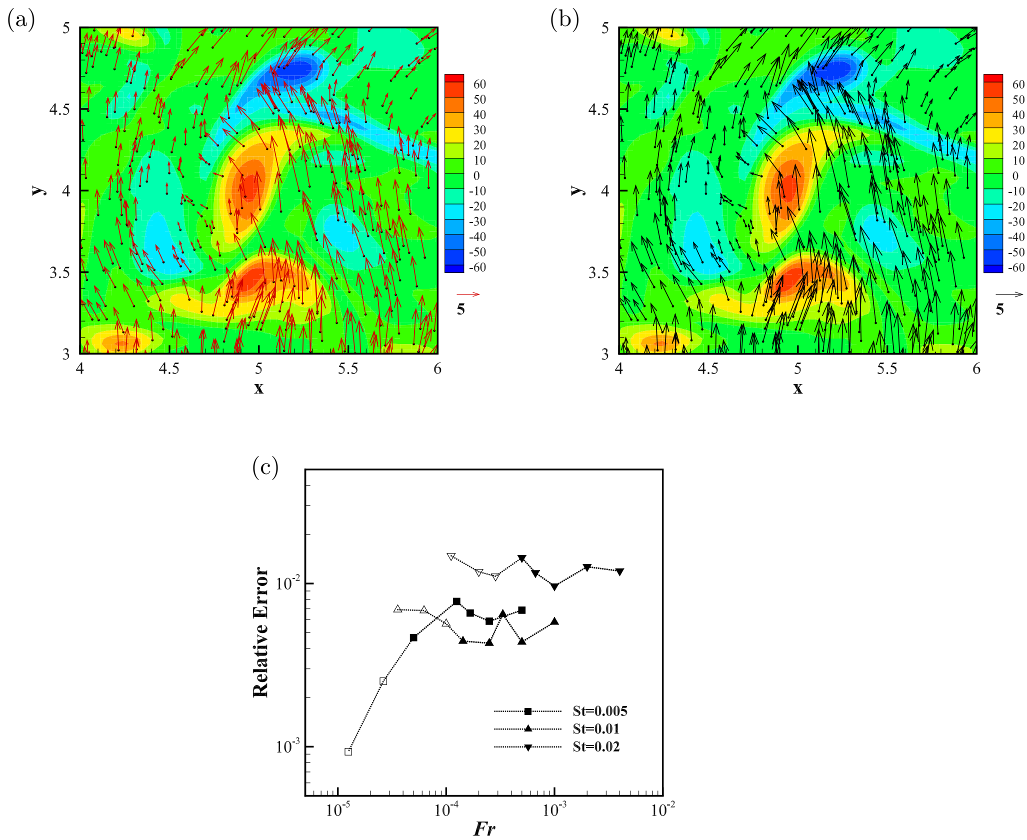

FIG. 1. Comparison of bubbles' velocity from (a) the full equation of motion [Eq. (1)] and (b) the weak form [Eq. (6)] and (c) the relative error between the two velocity fields defined by Eq. (7) in the same homogeneous isotropic turbulence. Here $\mathrm{St} = 0.005$ and $\mathrm{Fr} = 0.0005$. Color contours denote the vorticity component normal to the plane. Gravity acts downward and thus bubbles mostly rise. A bubble's position uniquely determines its velocity. Two velocity fields are identical even near strong vortices, confirming that the centripetal attraction of bubbles to the vortex cores is negligible. Open symbols in (c) correspond to cases with parameters outside the valid range $10^{-2}(6r)^{3/2} > \mathrm{Fr}\,\mathrm{St}^{-3/2}$ or $\mathrm{Re} > 100$, which will be discussed later.

The $(\boldsymbol{v}_g \cdot \nabla)\boldsymbol{u}$ term has zero compressibility and thus can be neglected. This can also be verified directly from the formulas for density statistics in weakly compressible flows provided below.

We see from Eq. (6) that the centripetal attraction of bubbles to the vortex cores is a minor effect in comparison with the much stronger effect of the lift force. That force produces a peculiar compressible component of the flow that has no vertical component yet depends on the vertical coordinate. Figure 1 confirms that the bubble velocities obtained by solving numerically the full equation of motion (1) and the approximated equation (6) are identical in the overdamped limit. The relative error E between the two bubble velocity fields illustrated in Fig. 1(c) is defined by

$$E \equiv \frac{\sqrt{\sum_j \left|\boldsymbol{v}_j^a - \boldsymbol{v}_j^b\right|^2}}{\sqrt{\sum_j \left|\boldsymbol{v}_j^a\right|^2}}, \tag{7}$$

where $\boldsymbol{v}_j^a$ and $\boldsymbol{v}_j^b$ are a bubble's velocity from the full equation of motion (1) and the weak form (6), respectively. It clearly indicates that on average the error between the two velocity fields is below 2% of the mean magnitude of the velocity field.

The existence of smooth bubbles' flow in the domain of validity of Eq. (1), which is given by Eq. (6), is the key result of our work. It immediately provides the reason for bubble clustering in downwelling flow. We have

$$\langle u_z \nabla \cdot \boldsymbol{v}\rangle = -2g\tau^2 \langle u_z \nabla^2 u_z\rangle = \frac{2g\tau^2\epsilon}{3\nu}, \tag{8}$$

where the angular brackets denote spatial averaging. We used the fact that the isotropy of small-scale turbulence implies that the work done by viscous forces $-\nu\langle u_z\nabla^2 u_z\rangle$ equals $\epsilon/3$. Thus, the vertical velocity in regions with negative $\nabla\cdot\boldsymbol{v}$ is predominantly negative. Because regions with $\nabla\cdot\boldsymbol{v} < 0$ attract tracers of flow $\boldsymbol{v}$, this demonstrates concentration in downwelling flow (see also the calculation of the cross correlation of u_z with the steady-state concentration below).

III. THE PK MODEL

The structure of the flow given by Eq. (6) is identical to the flow of spherical phytoplankton cells in the reduced PK model. In this section we introduce the PK model and this reduction. We also provide some results for aspherical cells that are outside the main scope of the paper, but are however relevant for the conclusions in Sec. VI.

The motion of a spherical cell in the PK model is described by the equations [23,24,26,27]

$$\frac{d\boldsymbol{x}}{dt} = \boldsymbol{u}[t,\boldsymbol{x}(t)] + \phi\hat{\boldsymbol{p}}(t), \quad \frac{d\hat{\boldsymbol{p}}}{dt} = \frac{\hat{\boldsymbol{k}} - (\hat{\boldsymbol{k}}\cdot\hat{\boldsymbol{p}})\hat{\boldsymbol{p}}}{2\psi} + \frac{\boldsymbol{\omega}\times\hat{\boldsymbol{p}}}{2}. \tag{9}$$

The velocity is the superposition of the turbulent flow at the position of the cell and the swimming velocity with constant magnitude ϕ. The swimming direction is described by the unit vector $\hat{\boldsymbol{p}}$ that changes in time due to the interplay of gravitaxis and the rotation due to the local vorticity [24,45]. A reorientation in the vertical direction due to the gravitaxis is described by the first term on the RHS, where $\hat{\boldsymbol{k}}$ is the unit vector in the upward direction and ψ is a constant timescale. In the absence of the last term on the RHS, $\hat{\boldsymbol{p}}$ would relax to $\hat{\boldsymbol{k}}$ on a timescale of order ψ. The last term on the RHS describes rotation with an angular velocity given by half the local vorticity $\boldsymbol{w} = \nabla\times\boldsymbol{u}$.

We consider the overdamped limit where the gravitaxis dominates changes in the swimming direction. This is the limit of $\psi\to 0$ where ψ is much less than both the Kolmogorov time of turbulence and the characteristic time η/ϕ during which the cells, drifting through the flow at velocity ϕ, cross the Kolmogorov scale η (for details see [23,26]). In that limit in the leading order, $\hat{\boldsymbol{p}} = \hat{\boldsymbol{k}}$, and we can neglect the time-derivative term in the equation for $\hat{\boldsymbol{p}}$. Writing $\hat{\boldsymbol{p}} = \hat{\boldsymbol{k}} + \delta\hat{\boldsymbol{p}}$, one can readily obtain the correction $\delta\hat{\boldsymbol{p}} = \psi\boldsymbol{\omega}\times\hat{\boldsymbol{k}}$. We find the reduced equation of motion [23]

$$\frac{d\boldsymbol{x}}{dt} = \boldsymbol{v}[t,\boldsymbol{x}(t)], \quad \boldsymbol{v} \equiv \boldsymbol{u} + (\phi\psi\omega_y, -\phi\psi\omega_x, \phi), \tag{10}$$

where we defined the flow of the microorganisms $\boldsymbol{v}(t,\boldsymbol{x})$. This reduces to Eq. (6) on letting $\phi = v_g$ and $\psi = \tau$. Thus, the theory for bubbles can be obtained by renaming the parameters of the theory of phytoplankton in turbulence [23,26]. We provide the results of this translation in the next section. Currently, we consider the possible role of the shape of the particles. This will only be needed in Sec. VI.

Role of the shape

Here we briefly consider the PK model for aspherical cells. This is not very relevant for the main course of this paper; however, it produces some results for this problem that are missing in the literature. The impact of the shape is described by introducing the strain term in Eq. (9) (see [24,27,28]):

$$\frac{d\boldsymbol{x}}{dt} = \boldsymbol{u}[t,\boldsymbol{x}(t)] + \phi\hat{\boldsymbol{p}}(t), \quad \frac{d\hat{\boldsymbol{p}}}{dt} = \frac{\hat{\boldsymbol{k}} - (\hat{\boldsymbol{k}}\cdot\hat{\boldsymbol{p}})\hat{\boldsymbol{p}}}{2\psi} + \frac{\boldsymbol{\omega}\times\hat{\boldsymbol{p}}}{2} + \Lambda[S\hat{\boldsymbol{p}} - \hat{\boldsymbol{p}}(\hat{\boldsymbol{p}}S\hat{\boldsymbol{p}})]. \tag{11}$$

The introduced last term describes the orienting action of the local strain described by the symmetric component S_{ik} of the tensor of velocity gradients $\nabla_k u_i$. The shape parameter Λ changes between zero, for spheres, and one, for rods. The correction to the vertical motion in the overdamped limit becomes $\delta\hat{\boldsymbol{p}} = \psi\boldsymbol{\omega}\times\hat{\boldsymbol{k}} + 2\psi\Lambda[S\hat{\boldsymbol{k}} - \hat{\boldsymbol{k}}(\hat{\boldsymbol{k}}S\hat{\boldsymbol{k}})]$. Thus, the reduced equation of motion in this case is

$$\frac{d\boldsymbol{x}}{dt} = \boldsymbol{v}[t,\boldsymbol{x}(t)],\quad \boldsymbol{v}\equiv\boldsymbol{u}+\phi\hat{\boldsymbol{k}}+\phi\psi[\omega_y+\Lambda(\nabla_z u_x+\nabla_x u_z),-\omega_x+\Lambda(\nabla_z u_y+\nabla_y u_z),0]. \tag{12}$$

This formula was obtained in [28]. The flow has a finite small compressibility $\nabla\cdot\boldsymbol{v} = -\phi\psi\nabla^2 u_z + \phi\psi\Lambda(\nabla_x^2+\nabla_y^2-\nabla_z^2)u_z$. A detailed study of the consequences is outside the scope of this work; see, however, the case of $\Lambda = 0$ in the next section. Here we only provide several results that are missing in [28]. It follows immediately from the theory of multifractal clustering developed in [12] that the cells obeying Eq. (12) are distributed in space over a multifractal attractor with Hentschel-Procaccia [46] generalized fractal dimensions $D(k) = 3 - C_{\mathrm{KY}}k$, where the Kaplan-Yorke codimension C_{KY} is

$$C_{\mathrm{KY}} = \frac{(\phi\psi)^2}{2|\lambda_3|}\int_{-\infty}^{\infty}\langle[\nabla^2 u_z(0)+\Lambda(\nabla_x^2+\nabla_y^2-\nabla_z^2)u_z(0)][\nabla^2 u_z(t)+\Lambda(\nabla_x^2+\nabla_y^2-\nabla_z^2)u_z(t)]\rangle dt, \tag{13}$$

where λ_3 is the third Lyapunov exponent of the fluid particles and the angular brackets denote the usual different time correlation functions of turbulence (see also [19]). The quadratic dependence on $\phi\psi$ was observed in [28]; here we provide the coefficient. The statistics of concentration n is log-normal with the pair-correlation function $\langle n(0)n(\boldsymbol{r})\rangle = \langle n\rangle^2(\eta/r)^{2C_{\mathrm{KY}}}$ at $r \ll \eta$. One can readily determine the average value of the vertical component of the turbulent velocity in the frame of the cell. Using the approach of [26], we have

$$\langle u_z[t,\boldsymbol{x}(t)]\rangle = -\int_{-\infty}^{0}\langle u_z(0)\nabla\cdot\boldsymbol{v}(t)\rangle dt = \phi\psi\int_{-\infty}^{0}\langle u_z(0)\nabla^2 u_z(t)\rangle dt + \phi\psi\Lambda\langle u_z(0) \times(\nabla_z^2-\nabla_x^2-\nabla_y^2)u_z(t)\rangle dt. \tag{14}$$

This average is negative; that is, the cells preferentially sample the regions of downwelling flow. For $\Lambda = 0$, this was demonstrated in [26]; for $\Lambda = 1$ (rods), this can be seen by similarly applying the considerations of [26] to

$$\langle u_z(t,\boldsymbol{x}(t),\Lambda=1)\rangle = 2\phi\psi\int_{-\infty}^{0}\langle u_z(0)\nabla_z^2 u_z(t)\rangle dt. \tag{15}$$

The sign of $\langle u_z(t,\boldsymbol{x}(t))\rangle$ can also be seen to be negative in the intermediate cases $0 < \Lambda < 1$. The prediction of preferential concentration in downwelling flow agrees with the numerical simulations of [28]. In contrast, [27] studied the expansion with respect to the Kubo number of the PK model in a Gaussian single-scale random flow. Those authors found that at large Λ the preferential concentration can be displaced to regions of upwelling flow. The simulations of [28] demonstrated that this occurs for fast elongated swimmers. These swimmers have a large ϕ and cannot be described by the overdamped limit. We will describe the role of shape in Sec. VI, returning for the moment to the spherical case.

IV. APPLYING ONE-TO-ONE CORRESPONDENCE WITH THE PK MODEL

The flow of bubbles is weakly compressible: From Eq. (6), $|\nabla\cdot\boldsymbol{v}|/|\nabla\boldsymbol{v}| \sim \tau/\tau_g \ll 1$. Thus, the statistics and structure of bubbles' concentration $n(\boldsymbol{x})$ in the steady state can be described using the theory of distribution of tracers in weakly compressible random flows [12] (see also [19,27,47]). In this section we describe the application of the theory adopted for the problem at hand.

From the general theory of smooth dynamical systems, we know that the steady-state concentration (the so-called natural measure) $n(\boldsymbol{x})$ of bubbles obeying the first of Eqs. (4) and Eq. (6) is a singular field. This field is supported on a multifractal attractor set X that changes continuously, keeping its space-averaged properties intact (see, e.g., [48,49] and the references therein). The problem of describing the set is generally unsolvable because it requires a detailed knowledge of the probability density function of finite-time Lyapunov exponents [49]. However, in the limit of weak compressibility (or weak dissipation in the language of dynamical systems), the problem admits a universal solution that is independent of the details of the flow in much the same way that the equilibrium statistical physics is independent of the details of microscopic interactions [12]. This result was obtained in a fluid mechanics context and is unknown in the theory of dynamical systems (cf. [48,50]).

If one solves the continuity equation

$$\partial_t n + \boldsymbol{v}\cdot\nabla n = -n\nabla\cdot\boldsymbol{v} \tag{16}$$

with an arbitrary smooth condition in the remote past, e.g., $n(t=-T)=\text{const}$, then in the steady-state limit of infinite evolution time $T\to\infty$ the steady-state concentration at $t=0$ is nonzero only on X. Because X has zero three-dimensional volume and $\int n(\boldsymbol{x})d\boldsymbol{x}$ is finite (providing the total number of particles), the steady-state concentration (called the natural measure) resembles a distribution of δ functions [48]. The spatial structure of fields of this type is studied using the finite coarse-grained concentration field $n_\varepsilon(\boldsymbol{x})$, which is finite in contrast to infinite or zero $n(\boldsymbol{x})$:

$$n_\varepsilon(\boldsymbol{x}) = \int_{|\boldsymbol{x}'-\boldsymbol{x}|<\varepsilon} n(\boldsymbol{x}')\frac{3d\boldsymbol{x}'}{4\pi\varepsilon^3}. \tag{17}$$

The concentration $n_\varepsilon(\boldsymbol{x})$ is the mass $m_\varepsilon(\boldsymbol{x})$ in a small ball of radius ε centered at $\boldsymbol{x}$ divided by the ball's volume. A rather simple result was demonstrated in [12]: The steady-state concentration n_ε is given by the solution of Eq. (16), which is rendered finite by cutting the evolution time T at a finite value t^*,

$$n_\varepsilon(\boldsymbol{x}) = n_0\exp\left(-\int_{-t^*}^{0}\nabla\cdot\boldsymbol{v}[\boldsymbol{q}(t,\boldsymbol{x}),t]dt\right), \tag{18}$$

where n_0 is the mean concentration, $\boldsymbol{q}(t,\boldsymbol{x})$ is the time t position of the bubble that passes through $\boldsymbol{x}$ at $t=0$ (the Lagrangian trajectory of $\boldsymbol{v}$), and the flow divergence $\nabla\cdot\boldsymbol{v}$ is given by Eq. (6). The time t^* is determined by the following condition: Bubbles that are concentrated at $t=0$ inside the ball of radius ε at time $-t^*$ fill an ellipsoid whose largest dimension is the Kolmogorov scale η. Then the mass inside the ball, which equals the mass of the initial ellipsoid, is given by the product of the ellipsoid's volume and n_0. This is because at small compressibility the fluctuations of concentration are strong only at the smallest scales and at scale η the concentration is uniform (see the details in [12]).

The time t^* can be written with the help of the so-called third Lyapunov exponent λ_3. Lagrangian evolution along the flow trajectories transforms a small ball with a size smaller than η into an ellipsoid whose smallest dimension shrinks exponentially fast with exponent $|\lambda_3|$ (see [51,52]). One finds that $t^*=|\lambda_3|^{-1}\ln(\eta/\varepsilon)$ (see [12]). The following is then readily seen from Eq. (18) [53],

$$\lim_{\varepsilon\to 0}\frac{\ln n_\varepsilon(\boldsymbol{x})}{\ln(\eta/\varepsilon)} = -\lim_{t^*\to\infty}\frac{1}{|\lambda_3|t_*}\int_{-t^*}^{0}\nabla\cdot\boldsymbol{v}[\boldsymbol{q}(t,\boldsymbol{x}),t]dt = -C_{\mathrm{KY}},\quad C_{\mathrm{KY}}\equiv\frac{\left|\sum_{i=1}^{3}\lambda_i\right|}{|\lambda_3|}, \tag{19}$$

where we introduced the backward-in-time sum of Lyapunov exponents

$$\sum_{i=1}^{3}\lambda_i = -\lim_{t\to\infty}\frac{1}{t}\int_{-t}^{0}\nabla\cdot\boldsymbol{v}[\boldsymbol{q}(t,\boldsymbol{x}),t]dt, \tag{20}$$

which is negative [54]. Here the limit is realization independent by application of the ergodic theorem [50] to the backward-in-time flow. The sum gives the backward-in-time logarithmic growth rate of an infinitesimal volume of bubbles, and due to the weakness of compressibility, it coincides with the forward-in-time sum [54]. The positive constant $C_{\rm KY}$ introduced in Eq. (19) coincides with the definition of the Kaplan-Yorke codimension [55] in the case of weak compressibility [29]. The codimension is determined by the Lyapunov exponents λ_i (discussed below), which is why $C_{\rm KY}$ is also called the Lyapunov codimension. It is given by

$$C_{\rm KY}=\frac{16g^2\tau^4\int_0^\infty E(k)k^3dk}{\int_0^\infty E(k)k\,dk}\sim\frac{16\,{\rm St}^4}{{\rm Fr}^2}\lesssim c\left(\frac{a}{\eta}\right)^2, \tag{21}$$

where $E(k)$ is the energy spectrum of turbulence, $c>10$, and ${\rm Fr}\gtrsim 10^{-2}(a/\eta)^3$ (see [12,26] and below). For a given flow, Fr is fixed and $C_{\rm KY}\propto a^8$, neglecting weak dependence via r. The inequality $C_{\rm KY}\ll 1$ that holds due to the weakness of compressibility implies that X fills the space quite densely. The mass contained in a ball of radius ε grows as $m_\varepsilon(\boldsymbol{x})\sim\varepsilon^{3-C_{\rm KY}}$ [see Eq. (19)], which is close to the growth law of smooth distributions $m_\varepsilon\sim\varepsilon^3$.

The limit in Eq. (19) is deterministic despite the fact that the bubbles are transported by the random turbulent flow. This can be traced to a form of the law of large numbers. The concentration decays to zero with the ball radius as $\varepsilon^{C_{\rm KY}}$. The formula holds for typical spatial points and does not hold for points on the attractor. The latter are described by another deterministic limit, for the information dimension, given by the Kaplan-Yorke formula [48,55]

$$\lim_{\varepsilon\to 0}\frac{\ln n_\varepsilon}{\ln(\eta/\varepsilon)}=C_{\rm KY}, \tag{22}$$

which holds for all $\boldsymbol{x}$ in X with the possible exception of points with zero total mass. This is consistent with Eq. (18), as seen from

$$\frac{1}{\ln(\eta/\varepsilon)}\int d\boldsymbol{x}\,n(\boldsymbol{x})\ln n_\varepsilon(\boldsymbol{x})=-\frac{1}{|\lambda_3|t^*}\int_{-t^*}^0 dt\int d\boldsymbol{x}\,n(\boldsymbol{x})\nabla\cdot\boldsymbol{v}[\boldsymbol{q}(t,\boldsymbol{x}),t]=C_{\rm KY}, \tag{23}$$

where we observed that by mass conservation the last spatial integral can be written as $\int d\boldsymbol{y}\,n(\boldsymbol{y})\nabla\cdot\boldsymbol{v}(\boldsymbol{y},t)$ with $\boldsymbol{y}=\boldsymbol{q}(t,\boldsymbol{x})$. We used the fact that an infinitesimal volume of tracers dV obeys $d\ln dV/dt=\nabla\cdot\boldsymbol{v}$ (see [56]), so the average logarithmic growth rate of an infinitesimal volume of particles $\sum_{i=1}^3\lambda_i$ equals $\langle n\nabla\cdot\boldsymbol{v}\rangle/n_0$.

Despite the fact that the set X' of points $\boldsymbol{x}$ on X for which Eq. (22) does not hold carries zero mass, $\int_{X'}n(\boldsymbol{x})d\boldsymbol{x}=0$, and this set is not at all negligible in applications where ε is finite due to a finite resolution scale. The reason is the intermittency of the statistics. The heart of the multifractality is that the concentration field scales in the ball radius with a space-dependent exponent

$$n_\varepsilon(\boldsymbol{x})=n_0\left(\frac{\varepsilon}{\eta}\right)^{\rho(\boldsymbol{x})}. \tag{24}$$

It is readily seen from that Eq. (18) that $\rho(\boldsymbol{x})$ has Gaussian statistics and therefore its probability density function (PDF) $P_\varepsilon(\rho)$ obeys

$$P_\varepsilon(\rho)=\frac{\sqrt{\ln(\eta/\varepsilon)}}{\sqrt{4\pi D_{KY}}}\left(\frac{\eta}{\varepsilon}\right)^{-(\rho-C_{\rm KY})^2/4C_{\rm KY}} \tag{25}$$

(see the details in [12,53]). Thus, the single point distribution of $n_\varepsilon(\boldsymbol{x})$ is log-normal [see Eq. (24)]. Gaussian integration yields

$$\langle n_\varepsilon^k\rangle=n_0^k\frac{\sqrt{\ln(\eta/\varepsilon)}}{\sqrt{4\pi C_{\rm KY}}}\int\left(\frac{\eta}{\varepsilon}\right)^{k\rho-(\rho-D_{\rm KY})^2/4C_{\rm KY}}d\rho\simeq n_0^k\left(\frac{\eta}{\varepsilon}\right)^{C_{\rm KY}k(k-1)}. \tag{26}$$

We see that because $C_{\rm KY}\ll 1$, we have $\langle n_\varepsilon^k\rangle\approx n_0^k$, unless ε is very small and/or $C_{\rm KY}$ is not that small. We see from Eq. (21) that the concentration fluctuations become strong for bubbles whose size is not very much smaller than η. At scales comparable to or larger than η, the coarse-grained concentration is uniform and there is no clustering. The fluctuations can become significant at small compressibility when compensated by the largeness of η/ε; cf. the similar situation for heavy inertial particles (see, e.g., [19]).

Bubble clustering in the downward flow side of the vortices [3,8] is described by the cross correlation $\langle u_z n\rangle$, where the fields are taken at the same point. Using the results of [26], one readily finds

$$\langle u_z n\rangle = -\frac{\pi}{2}\langle n\rangle\tau\int_0^\infty E(k)k\,dk. \tag{27}$$

This implies that the average rise velocity of the bubble takes the negative correction $\langle v_z\rangle = v_g - \pi\tau\int_0^\infty E(k)k\,dk/2$. This is found as the average of $\boldsymbol{u}$ in the bubble's frame [26] (see also [23,27,28,39]). The correction to v_g is Fr times smaller than v_g.

The above considerations were described in terms of the continuum description. We consider their implications for the motion of discrete bubbles. A single bubble in the flow would be found somewhere on the attractor, with $n_\varepsilon(\boldsymbol{x})$ giving the probability of being in the ε vicinity of $\boldsymbol{x}$. In the case of two bubbles, the PDF of the distance $\boldsymbol{r}$ between the particles is given by the RDF $g(\boldsymbol{r})$ that obeys

$$g(\boldsymbol{r}) = \frac{\langle n(0)n(\boldsymbol{r})\rangle}{n_0^2} = \left(\frac{\eta}{r}\right)^{2C_{\mathrm{KY}}}, \tag{28}$$

where it is readily seen that the scaling of $\langle n(0)n(\boldsymbol{r})\rangle$ in r coincides with that of $\langle n_r^2\rangle$ given by Eq. (26) (see [12,19,29]). The RDF at distances comparable to or larger than η is constant, manifesting lack of correlations of particles' positions at those distances. For two particles in volume Ω, the PDF of finding another particle at a distance $\boldsymbol{r}$ from one of the particles is $g(\boldsymbol{r})/\Omega$ and for $N+1$ independently moving bubbles the PDF is $g(\boldsymbol{r})N/\Omega$. The RDF is used to determine the collision kernel (see, e.g., [19]).

A deeper insight into the statistics of bubble clusters is obtained from the probability of finding N bubbles in a ball of radius ε. The deviations of this probability from the Poissonian prediction were used in an experimental study of bubble clustering [39]. The theoretical prediction for this probability was derived in [57], where it was demonstrated that the probability is doubly stochastic and given by a Poisson distribution with random intensity. The double stochasticity originates in the two-step formation of fluctuations with N particles within a radius ε. First, the particles are brought together from large distances under the scale η. The probability of this event is given by the Poisson distribution of independent particles, because beyond η the bubbles' motions do not correlate (or rather there is no increase in correlations beyond those of independent particles; the bubbles are in the same flow and their motions are correlated by the flow correlations in the inertial range). The next independent step of formation of a cluster of N particles inside a ball of radius ε consists of compression of the original volume with a size of order η inside the ball. The corresponding distribution is not trivial, and here we provide only the results of [57] for the second and third moments of the random number of particles N_ε inside the ball of radius ε. Using $\langle N_\varepsilon\rangle = 4\pi n_0\varepsilon^3/3$, the second moment is

$$\langle N_\varepsilon^2\rangle = \langle N_\varepsilon\rangle^2\left(\frac{\eta}{\varepsilon}\right)^{2C_{\mathrm{KY}}} + \langle N_\varepsilon\rangle. \tag{29}$$

This reduces to the Poissonian formula at nonsmall scales, for which $(\eta/\varepsilon)^{2C_{\mathrm{KY}}} \approx 1$. However, at smaller scales, there is indefinite growth of deviations from Poissonicity. These deviations quantify the clustering [57]. The continuum solutions provided previously are recovered in the limit $\langle N_\varepsilon\rangle \gg 1$. For the third moment, superposition of the power laws holds:

$$\frac{\langle N_\varepsilon^3\rangle}{\langle N_\varepsilon\rangle^3} = \left(\frac{\eta}{\varepsilon}\right)^{6D_{\mathrm{KY}}} + \frac{3}{\langle N_\varepsilon\rangle}\left(\frac{\eta}{\varepsilon}\right)^{2C_{\mathrm{KY}}} + \frac{1}{\langle N_\varepsilon\rangle^2} \tag{30}$$

(see the detailed treatment in [57]). Using this approach, one can consider the void probability of bubbles of a given size, which does not seem to be treatable in the continuum approach. Discreteness results in nontrivial phenomena [57].

The steady-state statistics of the spatial distribution of bubbles described above is completely determined by only one number: C_{KY}. That number is derived from the Lyapunov exponents [see Eq. (19)]. The exponents are interesting in their own right. These are defined [52] so that λ_1, $\lambda_1+\lambda_2$, and $\sum_{i=1}^{3}\lambda_i$ are the asymptotic logarithmic growth rates of an infinitesimal line, area, and volume elements, respectively. In the leading order [26]

$$\lambda_1\tau=-\lambda_3\tau=\frac{\pi}{16g}\int_0^\infty E(k)k\,dk\propto \mathrm{Fr},\quad |\lambda_2|\ll\lambda_1. \tag{31}$$

It is demonstrated in [26,29] that separation of infinitesimally close particles proceeds mainly horizontally. The vertical rising motion of the bubble causes a zero Lyapunov exponent in the vertical direction, similarly to how in time-independent systems displacement of the initial condition along the velocity direction causes no exponential separation [50]. Thus, the vertical component of the distance between the particles stays approximately constant. In contrast, the horizontal component grows exponentially with the positive exponent λ_1. Correspondingly, vertical configurations of bubbles are quasistationary: If random transport by the flow brings the particles above each other, they would stay in this configuration for much longer than in a similar horizontal configuration. As a result, the bubbles are seen to form columnar structures in space (cf. [29,58] and also [59]). For the sum of Lyapunov exponents [26] we have

$$\sum_{i=1}^{3}\lambda_i=-\pi g\tau^3\int_0^\infty E(k)k^3dk, \tag{32}$$

which is consistent with Eqs. (21) and (31).

V. NUMERICAL CONFIRMATION

In order to test the predictions, we performed a DNS of isotropic turbulence with laden bubbles. The Navier-Stokes equation was numerically solved on 128^3 grids using a spectral method in the periodic cubic domain to describe homogeneous isotropic turbulence at $\mathrm{Re}_\tau=67$. The integral length scale and the box size are 35η and 230η, respectively. The equation of bubble motion (1) was solved simultaneously. The details are found in [29,58,60–64]. The Lyapunov exponents are computed by releasing many pairs of particles. The initial distance between the particles is set to $10^{-8}\eta$ and the change in distance between two particles, the area between three particles, and the volume constructed from four particles are measured on the basis of Gram-Schmidt renormalization for a period of $30\tau_\eta$ after the transient period due to the arbitrary initial condition. There are 12 500 sets of pairs released in one flow field, and data are collected over a total of 15 flow fields.

The Lyapunov exponents λ_1 and λ_3 obtained from the DNS are compared with the theory in Fig. 2(a). In complete agreement with the theory, the data for different Stokes numbers collapse on the same curve in the range of validity of the model equation, $10^{-2}(6r)^{3/2}\lesssim \mathrm{Fr}\,\mathrm{St}^{-3/2}\lesssim(6r)^{3/2}$. The plots are log-log and they demonstrate that in all cases the power-law dependence on Fr is captured well by the theory. By contrast, for the coefficients, the agreement with the theory is limited. For instance, $\lambda_1\tau\propto \mathrm{Fr}$ describes the observations well, in accordance with Eq. (31); however, the proportionality constant differs from the prediction. We attribute this discrepancy to inaccuracy in the calculation of the moment of the energy spectrum with limited resolution. Deviations for large Fr might be caused by a numerical error in the prediction of small $\sum\lambda_i$ due to the cancellation between λ_1 and λ_3 ($\lambda_1\simeq-\lambda_3\sim \mathrm{Fr}$).

The Kaplan-Yorke codimension computed from the DNS is displayed with the theoretical estimates in Fig. 2(b). Agreement for $10^{-2}(6r)^{3/2}\lesssim \mathrm{Fr}\,\mathrm{St}^{-3/2}\lesssim(6r)^{3/2}$, which is the range of validity of Eq. (1) in terms of St and Fr, and even for the range outside the valid range is excellent.

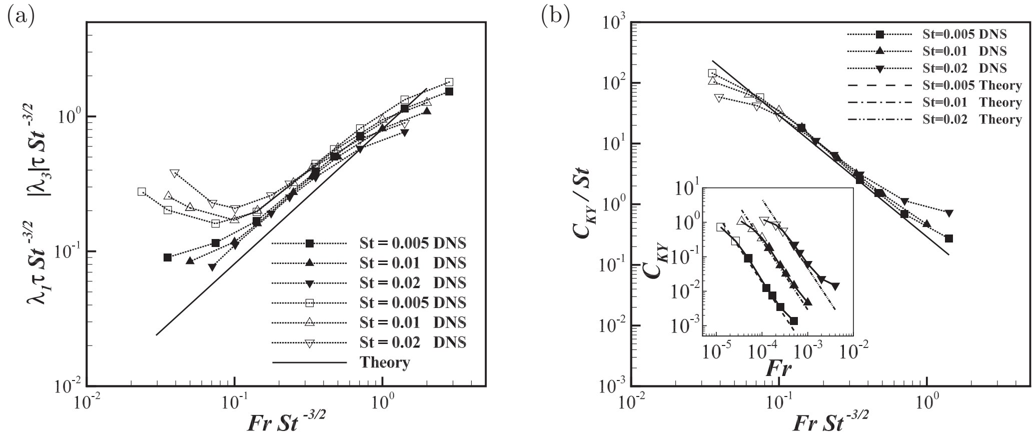

FIG. 2. Lyapunov exponents (a) $\lambda_1\tau$ (closed symbols) and $|\lambda_3|\tau$ (open symbols) and (b) Kaplan-Yorke codimension, obtained from the DNS (symbols) compared with theoretical estimates [lines, Eqs. (31) and (21)] for St $= 0.005$, 0.01, and 0.02. The Froude number and the Lyapunov exponents $\lambda_1\tau$ and $|\lambda_3|\tau$ are rescaled by $\mathrm{St}^{3/2}$ so that the range of validity of the model equation, $10^{-2}(6r)^{3/2} \lesssim \mathrm{Fr}\,\mathrm{St}^{-3/2} \lesssim (6r)^{3/2}$, is clearly shown. Here C_{KY} is compensated by St^4 and then rescaled by St^3 because the theory predicts $C_{\mathrm{KY}} \sim \mathrm{St}^4/\mathrm{Fr}^2$ [Eq. (21)]. Open symbols in (b) correspond to cases with parameters outside the valid range $10^{-2}(6r)^{3/2} > \mathrm{Fr}\,\mathrm{St}^{-3/2}$ or $\mathrm{Re} > 100$. The discrepancy for the upper rightmost point is due to $\tau_\eta/\tau_g \sim 5$ violating $\tau_\eta/\tau_g \gg 1$. The inset of (b) is provided for better reading of the value of C_{KY} for the given St and Fr.

The factors that determine the difference of the coefficients of λ_i from the theoretical predictions get compensated after the division and the theory holds.

In the range of validity of Eq. (1), the multifractal is quite dense in space, $D_{\mathrm{KY}} \ll 1$, and columns formed by bubbles are weakly pronounced. We also considered parameters at the limit of validity of the law of motion and of the theory, $a/\eta \lesssim 1$ and $\mathrm{Re} > 100$. We found a strong multifractal

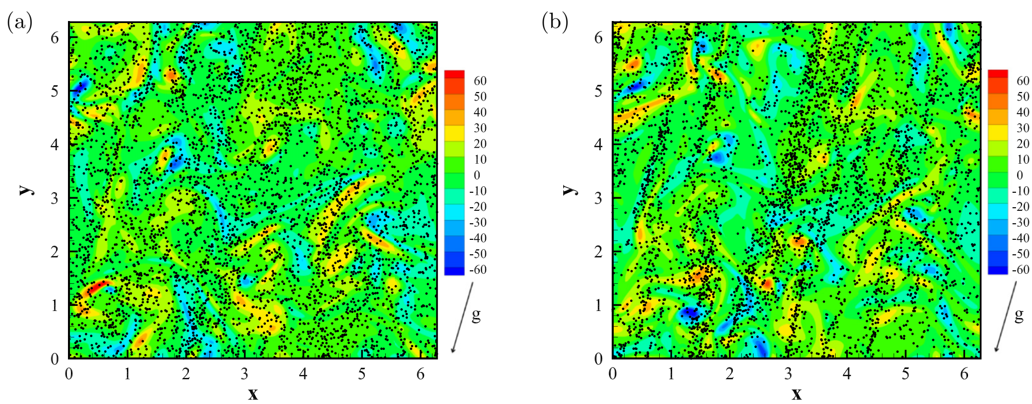

FIG. 3. Snapshot of bubble distribution for St $= 0.02$ and (a) Fr $= 0.0005$ ($\mathrm{Fr}\,\mathrm{St}^{-3/2} = 0.177$, $C_{\mathrm{KY}} = 0.222$); (b) Fr $= 0.0002$ ($\mathrm{Fr}\,\mathrm{St}^{-3/2} = 0.07$, $C_{\mathrm{KY}} = 0.845$). The color contour denotes the vorticity. The arrow below the colormap indicates the direction of gravity. The slightly slanted gravity direction is intentional to avoid numerical artifacts due to periodicity of flow fields. The parameters of case (a) satisfy the valid range $10^{-2}(6r)^{3/2}(\simeq 0.15) \lesssim \mathrm{Fr}\,\mathrm{St}^{-3/2} \lesssim (6r)^{3/2}$ ($\simeq$15), while those of case (b) are slightly outside the valid range, for which our theoretical prediction of the fractal dimension still shows good agreement with the simulation as shown in Fig. 2(b). The columnar structure of the bubbles is more pronounced, and the bubble clusters are more compressible as Fr decreases. Even for larger Fr, such a cluster is present, although it is not that pronounced.

structure with the fractal dimension significantly less than 3, as described by the leftmost points in Fig. 2(b). The bubbles form the columnar structure shown in Fig. 3(b) for parameters that correspond to $\mathrm{Re} > 350$ and $a/\eta \sim 0.6$. These parameters magnify preferential concentration in columns present in weaker form at $\mathrm{Re} \sim 105$ and $a/\eta \sim 0.5$, where the fractal dimension is small [Fig. 3(a)]. Theoretical formulas also work in these cases. The small error between the two velocity fields from the full equation of motion (1) and the weak form (6) for the parameters outside the valid range shown in Fig. 1(c) supports this. This implies, by asymptotic extension, that for bubbles with $a/\eta \sim 1$ and $\mathrm{Re} \gtrsim 100$ the fractality is strong and columns are robust. A quantitative description of these ranges requires deriving the law of motion there.

VI. CONCLUSION

In this work we derived an equation of motion for isolated bubbles 50–400 μm in size in turbulence. The equation is a reduction of the previously used model and holds for turbulence parameters typical in the ocean. The equation of motion has the same form as the equation for phytoplankton with a one-to-one correspondence of the motion parameters. We used this to formulate our theory of bubble distribution, which we confirmed by a DNS of the original nonreduced equation of motion of the bubble in Navier-Stokes turbulence.

Our reduction demonstrates that the centripetal acceleration of bubbles toward the cores of vortices $2\tau[\partial_t \boldsymbol{u} + (\boldsymbol{u} \cdot \nabla)\boldsymbol{u}]$, which is present in the equation of motion because the bubbles are light particles [11,12], is negligible in Eq. (4) in comparison compared with the lift term. The flow produced by the lift force increases the concentration of bubbles in downwelling flow. These facts, however, do not tell us anything about the correlation of the positions of the bubbles and vorticity. In fact, the simulations of [23] indicated that the PK model increases the concentration of tracers in vortex cores for laminar flow with a pair of counterrotating vortices. A similar increase has not been reported for turbulence and is yet to be observed. In fact, the increase in the mean settling velocity of heavy inertial particles in turbulence [59] would hint at a negative correlation between vorticity and downwelling flow: Inertial particles that are found predominantly outside vortices spend more time in downwelling flow. We could not find a theoretically calculable cross correlation between the concentration and vorticity. The question demands further, probably numerical, work that is beyond the scope of this paper.

Formation of bubble multifractals occurs by compression from the Kolmogorov scale to the scale of the bubble [12,26]. Its characteristic time is $\tau_\eta \ln(\eta/a)$, which does not exceed τ_η much. Thus, fractal formation occurs at the Kolmogorov temporal and spatial scales. At these times, our assumption that changes in the spherical shape of the bubbles can be disregarded is typically valid, implying that bubbles' multifractals are observable. For instance, the assumption of the spherical shape was observed to be true in [39].

Our derivation here relies on the equation of motion, whose validity strongly limits the range of the described parameters. The equation of motion employed requires the bubble size to be much smaller than the Kolmogorov scale of turbulence. This limits the theory to the case of very small Stokes numbers with $\mathrm{St}^{1/2} \ll 1$. At the same time, the experimental data demonstrate that both the preferential concentration and the change in the mean rise velocity are strongest at a Stokes number of order one (see, e.g., [39]). This is similar to the inertial particles in turbulence where clustering is also strongest at $\mathrm{St} \sim 1$ (see, e.g., [47]). Further progress requires an equation of motion for bubbles with a size comparable to the Kolmogorov scale of turbulence, where the Stokes number is of order one. The theory for this case is truly challenging due to the absence of scale separation between the scales of the particle and of the flow. Once this equation is obtained, it would also allow one to extend the range of the described Froude numbers. This is necessary to describe the change in the mean rise velocity observed in experiments [39].

One of the most interesting questions raised by our work is how far the correspondence between the motion of the bubbles and the PK model can be continued in terms of the parameters of the bubbles' motion. A consistent answer to this question requires the equation of motion of bubbles, which is not available today. However, new research questions arise if we assume as a working hypothesis that the correspondence can be continued at least qualitatively. It is known that besides the spherical shape considered here, the bubbles can also take the shapes of an ellipsoid and spherical cap as the size and Reynolds number increase [39,65]. At the same time, it was demonstrated that for the PK model, the change in the shape can bring about a qualitative change where clustering occurs in the upwelling regions of the flow and not in the downwelling regions [27,28]. The correspondence raises the question whether nonspherical bubbles could also cluster in the upwelling regions of the flow. This intriguing question is left for future work.

The experimental studies of [39] measured the preferential concentration of bubbles via the deviations of the PDF of the number of bubbles in a small volume from the Poisson distribution that holds for randomly distributed particles. The theory of these deviations for arbitrary weakly compressible flows was developed in [57]. The corresponding application of the theory to bubbles using the continuum flow derived in this work is straightforward.

We stress that the obtained theory for the bubbles is independent of the accuracy of the PK model for the description of phytoplankton. We use the solution of the PK equations irrespective of their origin. For instance, the average rise velocity of the actual motile phytoplankton cells could have corrections from inertial effects that the PK model disregards. Indeed, it was observed that turbulence also changes the average vertical (sedimentation) velocity of nonmotile phytoplankton microorganisms (see [66,67]). The effect was attributed mainly to the same inertial effects that change the average sedimentation velocity of rigid spheres in turbulence [59].

The discovered correspondence allows one to apply to bubbles the results of observations of phytoplankton in vortical motions [23] and density currents [68]. It also works in the opposite direction: Our prediction and observation of columnar structures of bubbles implies that similar structures must hold for phytoplankton. This exchange of data is possible as long as the validity of the PK model in describing the considered species can be assumed.

The described predictions for bubbles' distribution and movement in turbulence can be used for more effective inclusion of bubbles in numerical simulations of the ecology of the turbulent ocean.

ACKNOWLEDGMENT

This research was supported by Samsung Science & Technology Foundation (Grant No. SSTF-BA1702-03).

[1] P. L. Walls, J. C. Bird, and L. Bourouiba, Moving with bubbles: A review of the interactions between bubbles and the microorganisms that surround them, Integr. Comp. Biol. **54**, 1014 (2014).

[2] S. Sengupta and B. B. Jana, Effect of aeration on the primary productivity of phytoplankton in experimental tanks, Aquaculture **62**, 131 (1987).

[3] L.-P. Wang and M. R. Maxey, The motion of microbubbles in a forced isotropic and homogeneous turbulence, Appl. Sci. Res. **51**, 291 (1993).

[4] M. R. Maxey, E. J. Chang, and L.-P. Wang, Simulation of interactions between microbubbles and turbulent flow, Appl. Mech. Res. **47**, S70 (1994).

[5] P. D. M. Spelt and A. Biesheuvel, On the motion of gas bubbles in homogeneous isotropic turbulence, J. Fluid Mech. **336**, 221 (1997).

[6] M. R. Maxey, B. K. Patel, E. J. Chang, and L.-P. Wang, Simulations of dispersed turbulent multiphase flow, Fluid Dyn. Res. **20**, 143 (1997).

[7] I. M. Mazzitelli, D. Lohse, and F. Toschi, The effect of microbubbles on developed turbulence, Phys. Fluids **15**, L5 (2003).

[8] I. M. Mazzitelli, D. Lohse, and F. Toschi, On the relevance of the lift force in bubbly turbulence, J. Fluid Mech. **488**, 283 (2003).

[9] M. R. Snyder, O. M. Knio, J. Katz, and O. P. Le Maitre, Statistical analysis of small bubble dynamics in isotropic turbulence, Phys. Fluids **19**, 065108 (2007).
[10] E. Calzavarini, M. Cencini, D. Lohse, and F. Toschi, Quantifying Turbulence-Induced Segregation of Inertial Particles, Phys. Rev. Lett. **101**, 084504 (2008).
[11] E. Calzavarini, M. Kerscher, D. Lohse, and F. Toschi, Dimensionality and morphology of particle and bubble clusters in turbulent flow, J. Fluid Mech. **607**, 13 (2008).
[12] I. Fouxon, Distribution of Particles and Bubbles in Turbulence at a Small Stokes Number, Phys. Rev. Lett. **108**, 134502 (2012).
[13] J. M. Mercado, V. N. Prakash, Y. Tagawa, C. Sun, and D. Lohse, Lagrangian statistics of light particles in turbulence, Phys. Fluids **24**, 055106 (2012).
[14] T. R. Auton, The lift force on a spherical body in a rotational flow, J. Fluid Mech. **183**, 199 (1987).
[15] D. Legendre and J. Magnaudet, The lift force on a spherical bubble in a viscous linear shear flow, J. Fluid Mech. **368**, 81 (1998).
[16] L. Biferale, F. Bonaccorso, I. M. Mazzitelli, M. A. T. van Hinsberg, A. S. Lanotte, S. Musacchio, P. Perlekar, and F. Toschi, Coherent Structures and Extreme Events in Rotating Multiphase Turbulent Flows, Phys. Rev. X **6**, 041036 (2016).
[17] A. M. Kamp, A. K. Chesters, C. Colin, and J. Fabre, Bubble coalescence in turbulent flows: A mechanistic model for turbulence-induced coalescence applied to microgravity bubbly pipe flow, Int. J. Multiphase Flow **27**, 1363 (2001).
[18] M. R. Maxey, The gravitational settling of aerosol particles in homogeneous turbulence and random flow fields, J. Fluid Mech. **174**, 441 (1987).
[19] G. Falkovich, A. Fouxon, and M. G. Stepanov, Acceleration of rain initiation by cloud turbulence, Nature (London) **419**, 151 (2002).
[20] M. Wilkinson and B. Mehlig, Caustics in turbulent aerosols, Europhys. Lett. **71**, 186 (2005).
[21] G. Falkovich and A. Pumir, Sling effect in collisions of water droplets in turbulent clouds, J. Atmos. Sci. **64**, 4497 (2007).
[22] E. W. Saw, G. P. Bewley, E. Bodenschatz, R. S. Sankar, and J. Bec, Extreme fluctuations of the relative velocities between droplets in turbulent airflow, Phys. Fluids **26**, 111702 (2014).
[23] W. M. Durham, E. Climent, M. Barry, F. De Lillo, G. Boffetta, M. Cencini, and R. Stocker, Turbulence drives microscale patches of motile phytoplankton, Nat. Commun. **4**, 2148 (2013).
[24] T. J. Pedley and J. O. Kessler, Hydrodynamic phenomena in suspensions of swimming microorganisms, Annu. Rev. Fluid Mech. **24**, 313 (1992).
[25] F. De Lillo, M. Cencini, W. M. Durham, M. Barry, R. Stocker, E. Climent, and G. Boffetta, Turbulent Fluid Acceleration Generates Clusters of Gyrotactic Microorganisms, Phys. Rev. Lett. **112**, 044502 (2014).
[26] I. Fouxon and A. Leshansky, Phytoplankton's motion in turbulent ocean, Phys. Rev. E **92**, 013017 (2015).
[27] K. Gustavsson, F. Berglund, P. R. Jonsson, and B. Mehlig, Preferential Sampling and Small-Scale Clustering of Gyrotactic Microswimmers in Turbulence, Phys. Rev. Lett. **116**, 108104 (2016).
[28] M. Borgnino, G. Boffetta, F. De Lillo, and M. Cencini, Gyrotactic swimmers in turbulence: Shape effects and role of the large-scale flow, J. Fluid Mech. **856**, R1 (2018).
[29] I. Fouxon, Y. Park, R. Harduf, and C. Lee, Inhomogeneous distribution of water droplets in cloud turbulence, Phys. Rev. E **92**, 033001 (2015).
[30] A. M. Balk, G. Falkovich, and M. G. Stepanov, Growth of Density Inhomogeneities in a Flow of Wave Turbulence, Phys. Rev. Lett. **92**, 244504 (2004).
[31] M. Vucelja, G. Falkovich, and I. Fouxon, Clustering of matter in waves and currents, Phys. Rev. E **75**, 065301 (2007).
[32] M. Vucelja and I. Fouxon, Weak compressibility of surface wave turbulence, J. Fluid Mech. **593**, 281 (2007).
[33] L. Schmidt, I. Fouxon, D. Krug, M. van Reeuwijk, and M. Holzner, Clustering of particles in turbulence due to phoresis, Phys. Rev. E **93**, 063110 (2016).
[34] N. Khurana and N. T. Ouellette, Stability of model flocks in turbulent-like flow, New J. Phys. **15**, 095015 (2013).

[35] A. Choudhary, D. Venkataraman, and S. S. Ray, Effect of inertia on model flocks in a turbulent environment, Europhys. Lett. **112**, 24005 (2015).
[36] A. W. Baggaley, Model flocks in a steady vortical flow, Phys. Rev. E **91**, 053019 (2015).
[37] J. Happel and H. Brenner, *Low Reynolds Number Hydrodynamics: With Special Applications to Particulate Media* (Springer Science + Business Media, New York, 2012).
[38] V. G. Levich, *Physicochemical Hydrodynamics* (Advance, New York, 1977).
[39] A. Aliseda and J. C. Lasheras, Preferential concentration and rise velocity reduction of bubbles immersed in a homogeneous and isotropic turbulent flow, Phys. Fluids **23**, 093301 (2011).
[40] T. R. Auton, J. C. R. Hunt, and M. Prud'Homme, The force exerted on a body in inviscid unsteady non-uniform rotational flow, J. Fluid Mech. **197**, 241 (1988).
[41] M. R. Maxey, The motion of small spherical particles in a cellular flow field, Phys. Fluids **30**, 1915 (1987).
[42] U. Frisch, *Turbulence: The Legacy of A. N. Kolmogorov* (Cambridge University Press, Cambridge, 1995).
[43] H. Medwin, *In situ* acoustic measurements of bubble populations in coastal ocean waters, J. Geophy. Res. **75**, 599 (1970).
[44] J. Wu, Bubbles in the near-surface ocean: A general description, J. Geophys. Res. **93**, 587 (1988).
[45] L. G. Leal and E. J. Hinch, The rheology of a suspension of nearly spherical particles subject to Brownian rotations, J. Fluid Mech. **55**, 745 (1972).
[46] H. G. E. Hentschel and I. Procaccia, The infinite number of generalized dimensions of fractals and strange attractors, Physica D **8**, 435 (1983).
[47] J. Bec, Fractal clustering of inertial particles in random flows, Phys. Fluids. **15**, L81 (2003).
[48] Ya. Pesin, *Dimension Theory in Dynamical Systems* (University of Chicago Press, Chicago, 1997).
[49] J. Bec, K. Gawedzki, and P. Horvai, Multifractal Clustering in Compressible Flows, Phys. Rev. Lett. **92**, 224501 (2004).
[50] J. R. Dorfman, *An Introduction to Chaos in Nonequilibrium Statistical Mechanics* (Cambridge University Press, Cambridge, 1999).
[51] E. Balkovsky and A. Fouxon, Universal long-time properties of Lagrangian statistics in the Batchelor regime and their application to the passive scalar problem, Phys. Rev. E **60**, 4164 (1999).
[52] G. Falkovich, K. Gawedzki, and M. Vergassola, Particles and fields in fluid turbulence, Rev. Mod. Phys. **73**, 913 (2001).
[53] I. Fouxon, Inertial particles in turbulence: New, robust results, online lecture course, available at https://sites.google.com/site/itzhakfouxonphd/teaching/inertial-particles-in-turbulence-course.
[54] I. Fouxon, Evolution to a singular measure and two sums of Lyapunov exponents, J. Stat. Mech. (2011) L02001.
[55] J. L. Kaplan and J. A. Yorke, in *Functional Differential Equations and Approximations of Fixed Points*, edited by H. O. Peitgen and H. O. Walther (Springer, Berlin, 1979), p. 204.
[56] G. K. Batchelor, *An Introduction to Fluid Dynamics* (Cambridge University Press, Cambridge, 2000).
[57] L. Schmidt, I. Fouxon, and M. Holzner, Inertial particles distribute in turbulence as Poissonian points with random intensity inducing clustering and supervoiding, Phys. Rev. Fluids **2**, 074302 (2017).
[58] Y. Park and C. Lee, Gravity-driven clustering of inertial particles in turbulence, Phys. Rev. E **89**, 061004(R) (2014).
[59] L.-P. Wang and M. R. Maxey, Settling velocity and concentration distribution of heavy particles in homogeneous isotropic turbulence, J. Fluid Mech. **256**, 27 (1993).
[60] S. Lee and C. Lee, Intermittency of acceleration in isotropic turbulence, Phys. Rev. E **71**, 056310 (2005).
[61] J. Jung, K. Yeo, and C. Lee, Behavior of heavy particles in isotropic turbulence, Phys. Rev. E **77**, 016307 (2008).
[62] Y. Choi, B.-G. Kim, and C. Lee, Alignment of velocity and vorticity and the intermittent distribution of helicity in isotropic turbulence, Phys. Rev. E **80**, 017301 (2009).
[63] A. H. Abdelsamie and C. Lee, Decaying versus stationary turbulence in particle-laden isotropic turbulence: Turbulence modulation mechanism, Phys. Fluids **24**, 015106 (2012).
[64] A. H. Abdelsamie and C. Lee, Decaying versus stationary turbulence in particle-laden isotropic turbulence: Heavy particle statistics modifications, Phys. Fluids **25**, 033303 (2013).
[65] R. Clift, J. R. Grace, and M. E. Weber, *Bubbles, Drops, and Particles* (Courier, Chelmsford, 2005).

[66] J. Ruiz, D. Macías, and F. Peters, Turbulence increases the average settling velocity of phytoplankton cells, Proc. Natl. Acad. Sci. USA **101**, 17720 (2004).

[67] C. Marchioli, M. Fantoni, and A. Soldati, Influence of added mass on anomalous high rise velocity of light particles in cellular flow field: A note on the paper by Maxey (1987), Phys. Fluids **19**, 098101 (2007).

[68] F. Liu, L. Zeng, Y. H. Wu, B. Baoligao, and X. Chen, Vertical distribution of motile phytoplankton in density currents, IOP Conf. Ser.: Earth Environ. Sci. **82**, 012073 (2017).